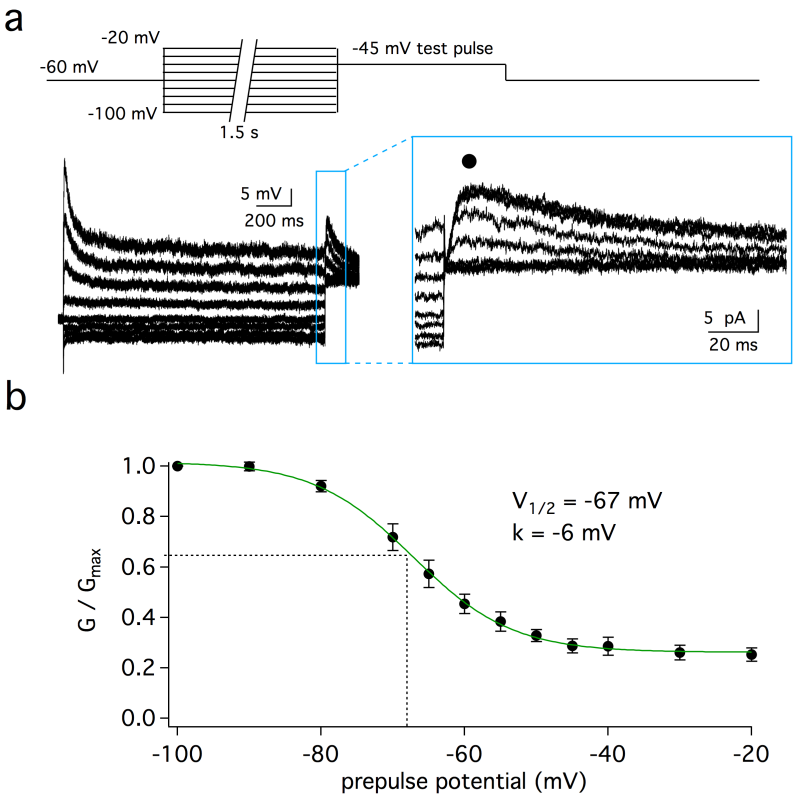

Supplementary Figure 1. Steady-state inactivation of $I_{K\text{-}LVA}$ in outside-out patches pulled from the soma of MSO principal neurons (25°C).
a. Tail currents were measured (circle, right expanded traces) at -45 mV following1.5s prepulses to voltages between -100 mV to -20 mV in 5 or 10 mV steps.
b. Normalized conductance plot of steady-state inactivation.The relationship is fit with a Boltzmann function (green), which exhibits a half-activation voltage of -67 mV and a slope (k) of -6 mV. Note that 26% of the peak current is non-inactivating.

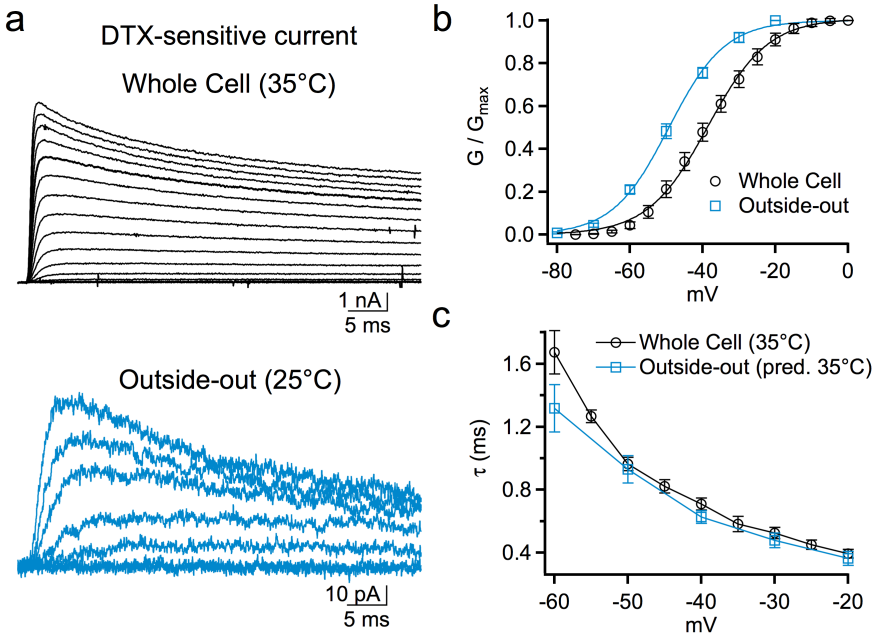

Supplementary Figure 2. Comparison of $I_{K\text{-}LVA}$ in measurements from whole-cell recordings vs. outside-out patches. **a.** The voltage of half activation is ~11 mV more hyperpolarized in outside-out vs whole-cell recordings. DTX-sensitive current responses to a family of square voltage steps between –80 and 0 mV. Holding potentials were –80 mV in whole-cell and –90 mV in outside-out recordings. **b.** Peak conductance-voltage plots illustrate the –11 mV shift in the voltage of half activation in outside-out (V1/2= -49.0 ± 1.5 mV, k= 7.4 ± 0.7) versus whole-cell ($V_{1/2}$ = -37.6 ± 1.6 mV, k= 8.8 ± 0.5) recordings. **c.** The rates of activation that were predicted for outside-out patches near physiological temperature (currents at 25°C corrected for 35°C using an experimentally measured Q_{10} of 3.3) correspond well with those in whole-cell recordings obtained at 35°C.

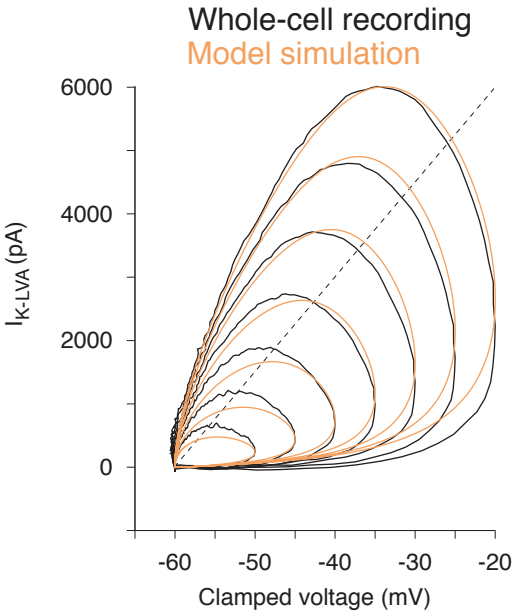

Supplementary Figure 3: Interplay between voltage and $I_{K\text{-}LVA}$ dynamics. Loops made with voltage versus $I_{K\text{-}LVA}$ time courses from whole-cell recordings (black, Fig. 5) and computer simulation (orange) on a EPSP-shape voltage clamp configuration. This representation of the time courses shows that the model not only reproduces the total amount of recruited $I_{K\text{-}LVA}$ for a particular voltage depolarization but also the particular time evolution and delays between voltage and active current dynamics. Possible reason for small discrepancy is due the leak sustraction on the whole cell recording experiment that could eliminate the voltage independent component from $I_{K\text{-}LVA}$ that is present in the model counterpart. Discontinuous line represents the shape of the relationship between voltage and an hypotetical leakeage current. Simulated responses were computed with step-gradient compartmental model; this whole cell current includes $I_{K\text{-}LVA}$ in soma and leak-subtracted current that flows to dendrite of neuron model.

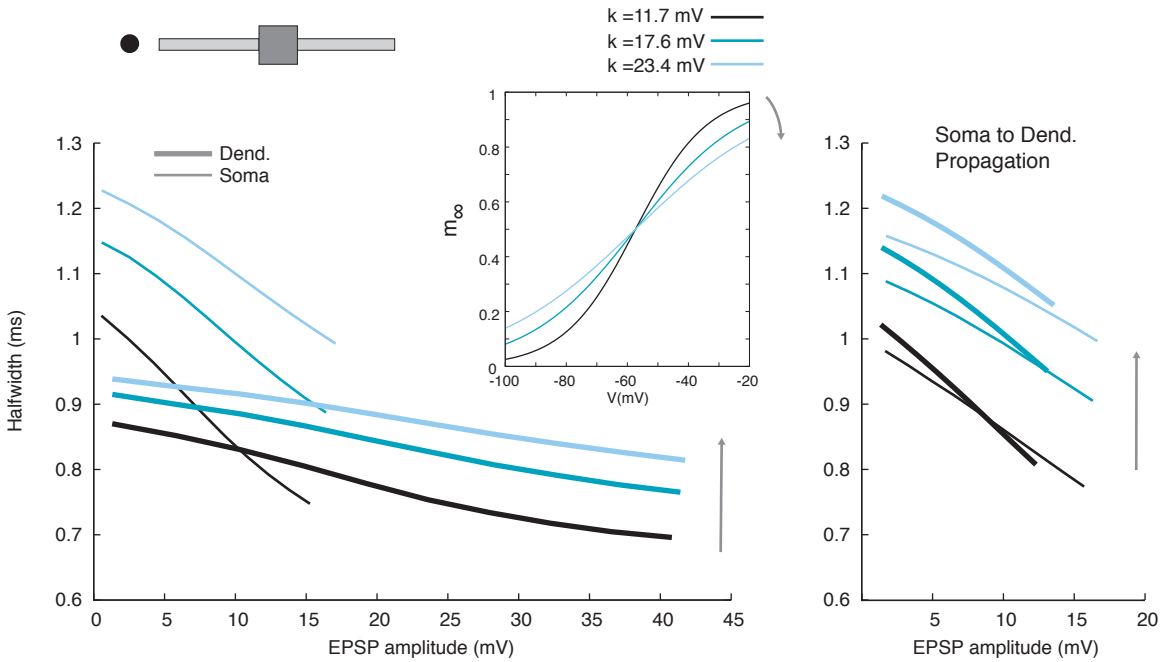

Supplementary Figure 4: Step-gradient model showing the dependence of VDS on the slope of the $I_{K\text{-}LVA}$ activation function, $m_\infty(V)$. Left and right panels display EPSP halfwidths for dendritic and somatic sites of current injection, respectively. Left, inset: Activation function "$m_\infty(V)$" for $I_{K\text{-}LVA}$ for the same half activation value $V_{1/2,m}$ but different slopes (proportional to $1/k_m$), see Methods. The model for $g_{K\text{-}LVA}$ (= $G_{K\text{-}LVA}.m_\infty^4 h$) dynamics was fit to voltage-clamp data using the program Neurofit. The value of k_m was also considered subsequently as a parameter in seeking the best match to the VDS data, yielding the value k_m= 11.7 mV, which agreed with whole-cell voltage clamp data. The shallower sloped m functions led to EPSP halfwidths that were too large and inadequate VDS rates.

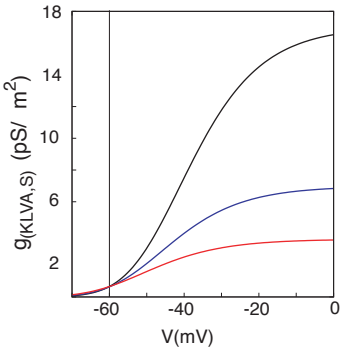

Supplementary Figure 5: Constraint on conductance ($G_{K\text{-}LVA}$) amplitude in the model for different $V_{1/2}$ of $I_{K\text{-}LVA}$ activation in order to satisfy V_{rest} = -60 mV (dendrite/soma density ratio is about 0.2). These three gating functions ($G_{K\text{-}LVA}.m^4_\infty h$) were used in simulations in Fig 6c. If the amount of $G_{K\text{-}LVA}$ is increased at rest, then the amount of G_h must also be increased at its resting value in order to maintain the equivalent driving forces to keep V_{rest}=-60mV. When the $V_{1/2}$ is shifted towards more hyperpolarized voltages, the amount of active current would increase twice us much due to the increment also in G_h needed to mantain the V_{rest}= -60 mV. This would increase the membrane time constant at rest. Therefore, changes in $V_{1/2}$ must be compensated by changes in $G_{K\text{-}LVA}$ to keep V_{rest} and the membrane time constant unchanged (from black to red curves).

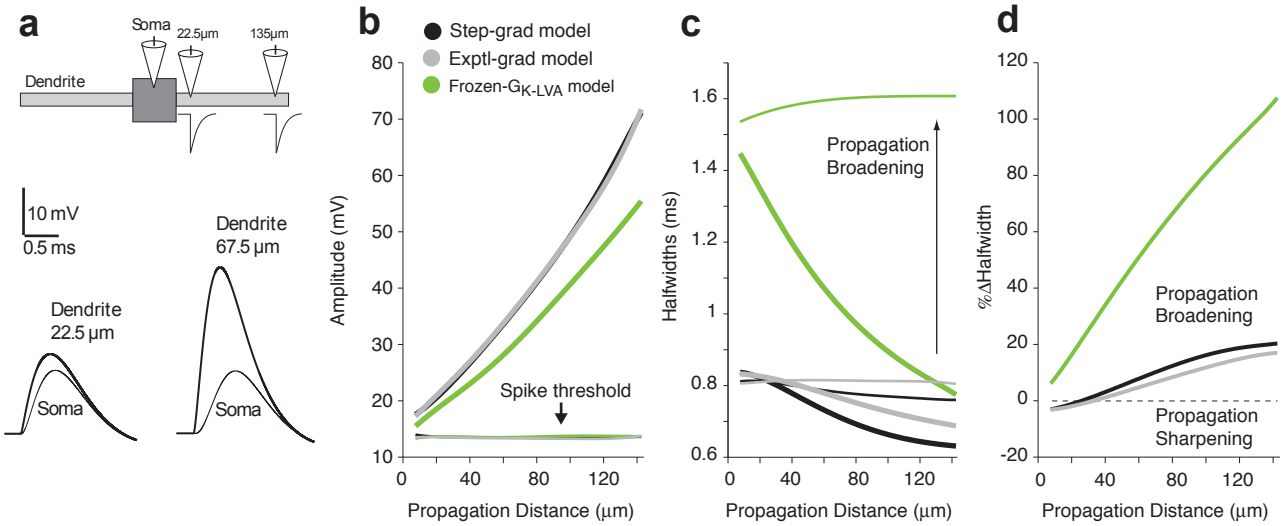

Supplementary Figure 6: The active properties of $I_{K\text{-}LVA}$ ensure uniform half-width for somatic EPSPs after propagation from different dendritic input locations. **a.** Top: schematic of step-gradient-density neuron model with one proximal and one distal current input injection. Below: example EPSP traces produced by proximal or distal dendritic EPSC injection in the step-gradient-density neuron model. Membrane time constants were set at 0.6 ms and 1.6ms for soma and dendrites respectively. **b.** EPSP peak response to current injection input is plotted for the dendritic (local) and somatic (propagated) locations (**Note:** current input strength was adjusted to maintain somatic response at 13mV for all stimulus locations). Simulations correspond to experiments in Fig 2b. As predicted by cable theory EPSP amplitude attenuates from stimulus location to the soma. Different cases show that exponential-gradient and step-gradient models give similar attenuation results while frozen $g_{K\text{-}LVA}$ case shows a bit less attenuation. **c.** Halfwidths of EPSP responses, dendritic (local) and somatic (propagated) were plotted against input locations. When $g_{K\text{-}LVA}$ is frozen local EPSP responses are broader locally and suffer more extensive broadening than when $g_{K\text{-}LVA}$ is active and shapes the response. Somatic EPSP halfwidth is nearly constant for different input locations in the case of active $g_{K\text{-}LVA}$ (see also Fig 2c for comparison). **d.** Halfwidth ratio (soma/dendrite) in percentage for different current injection locations. Exponential gradient $I_{K\text{-}LVA}$ distribution shows the smallest broadening effect on propagated EPSPs (See also Fig 3g for comparison).

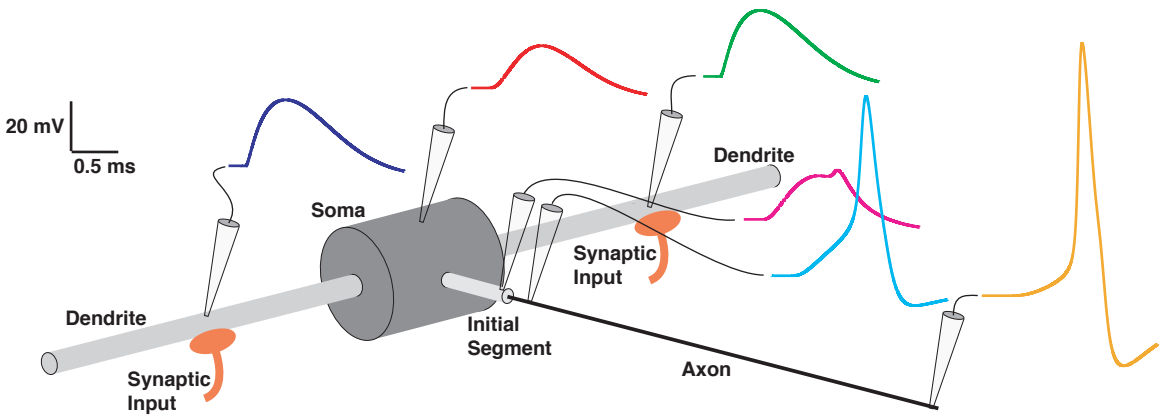

Supplementary Figure 7: Multicompartment model that includes spike generation compartments. The model retains the same soma and dendrite compartments as in the other simulations with the addition of a initial segment compartment and an axon compartment. The resting potential in all the compartments is -60mV. Initial segment and axon compartments have high threshold potassium current and sodium current as the only active currents present. Synaptic inputs were injected into the fifth compartment on both dendrites in order to mimic ITD-like inputs; time courses of EPSPs at the input sites are shown in green and blue. The summation of bilateral inputs leads to the somatic EPSP (red). The EPSP recorded at the distal compartment of the initial segment is plotted in pink. This EPSP exhibits a late brief small deflection, the attenuated back-propagated perturbation generated by the spike in the axon. There is no evidence of the axonal-generated spike back-propagating to the soma in this model. This might also be an important feature of the $I_{K\text{-}LVA}$ in MSO neurons creating a nearly pure feed-forward computation system. Outputs from the MSO neurons will not affect the sensitivity to the time precision on the bilateral inputs of this nerve cell. For our ITD tuning curve simulations we computed the number of spikes in the initial part of the axon (light blue curve). We utilized several axonal compartments to ensure that spikes successfully propagated forward along the axon and that spike generation at the proximal region of the axon was not inuenced by the boundary condition at the axon's distal end.

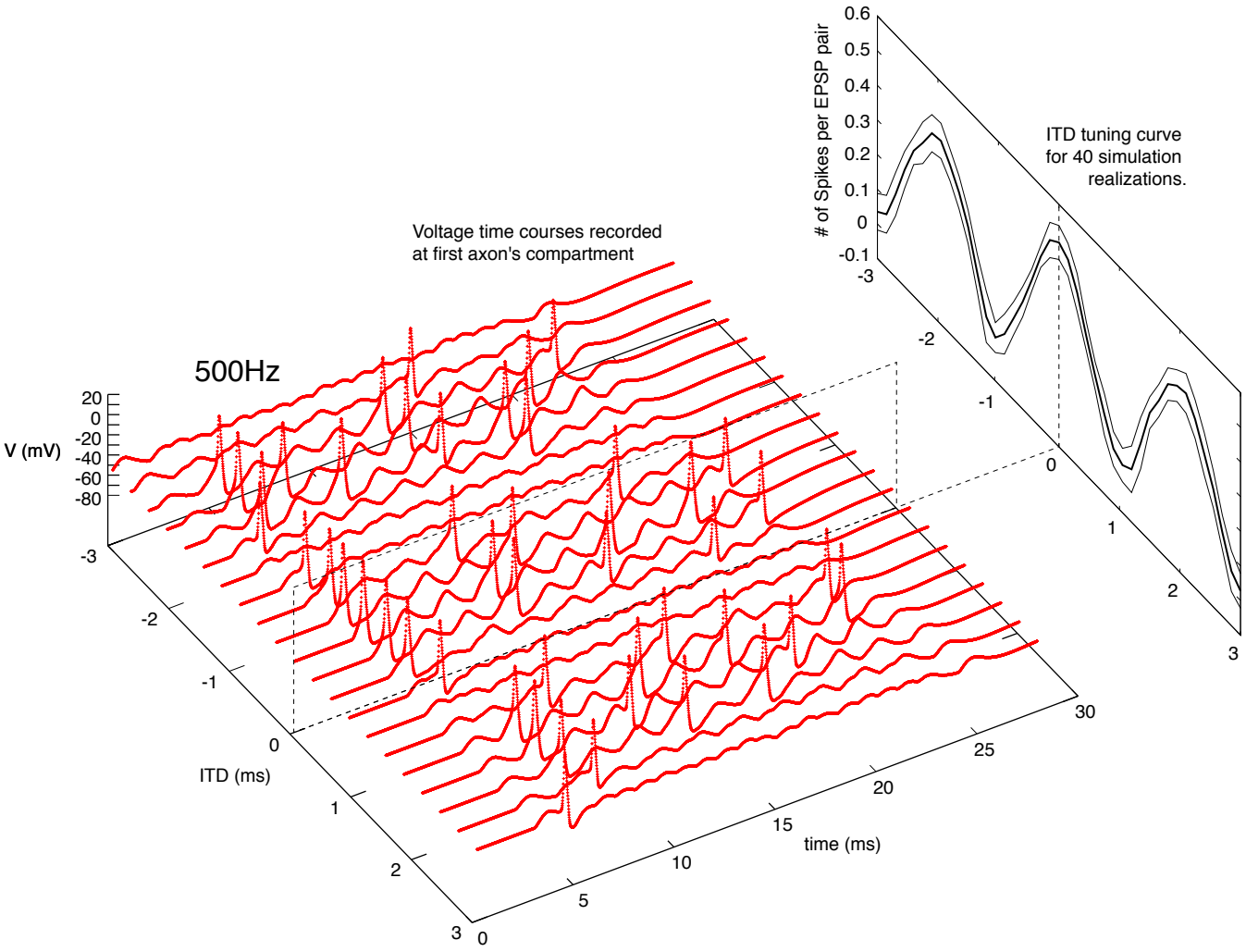

Supplementary Figure 8: ITD tuning curve generated by counting the number of spikes per bilateral EPSP-pair in the axon's first segment for the multicompartment model (see Methods and Suppl. Fig. 7). Each simulation realization for a particular ITD has 10 cycles of synaptic input injected in the dendrites. Synaptic inputs are conductance transients (alpha functions) with gaussian distribution in their amplitudes around some non-zero average. Halfwidth of EPSGs were adjusted cycle by cycle in order to have the same total (time integral) conductance while their amplitude is randomly generated; each EPSG is considered to be an idealization of the composite unitary EPSGs with jitter from the ipsilateral and contralateral afferents. Left, in red are the voltage time courses for different ITDs for a single realization. Right, ITD tuning curve from counting spikes per EPSP-pair for 40 realizations for each ITD value. Thick curve is the average number of spikes, thin curve corresponds to +/- one standard deviation. **Note:** standard deviation is smaller on the sides of the ITD tuning curve than around the peaks or troughs.

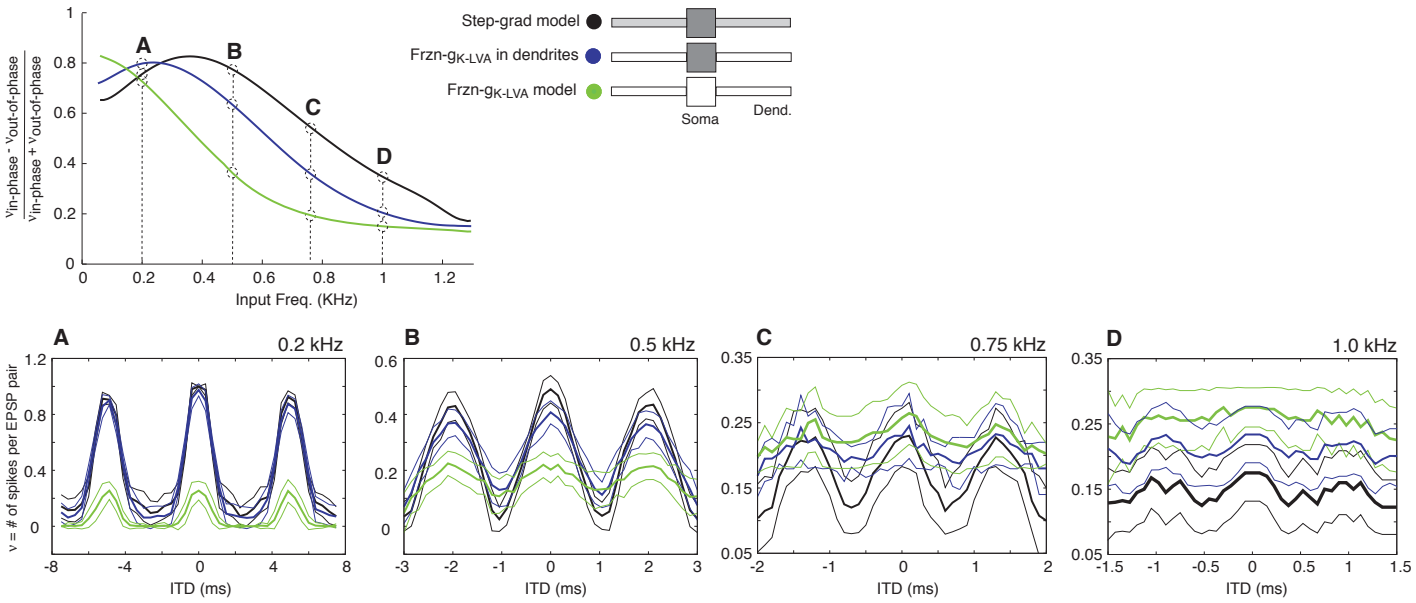

Supplementary Figure 9: ITD tuning curve sensitivity to different input frequencies. Top row, the model with no active $g_{K\text{-}LVA}$ (green curve) shows a decreasing monotonic dependence with frequencies starting at maximum sensitivity only for very low inputs frequencies. Sensitivity to ITD increases with the amount of dynamic (non-frozen) $g_{K\text{-}LVA}$ in the neuron model. If $g_{K\text{-}LVA}$ is active in the soma compartment only (blue curve) there is an increase in sensitivity with respect to the previous model. The higher sensitivity for the largest input frequency range is realized when $g_{K\text{-}LVA}$ is also active in the dendrites. Bottom row, ITD tuning curve generated for 4 particular examples of input frequency: 0.2, 0.5, 0.75 and 1.0 kHz. Thick curves are the average number of spikes for each ITD input and the thin lines are for +/- one standard deviation. The loss in sensitivity for higher fequencies is a combination of decrease in firing rate for inputs in-phase (ITD tuning curve peaks) but also a relative increase in firing rate for inputs out-of-phase (ITD tuning curve troughs). In a coding scheme framework the increase in spike number for out-of-phase inputs corresponds to scoring too many false positive responses.

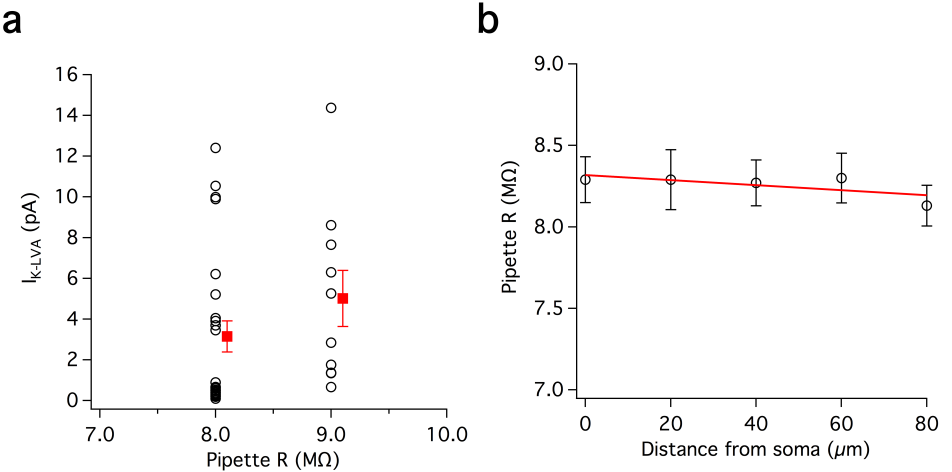

Supplementary Figure 10. K^+ current amplitude is not correlated with pipette resistance. **a.** Peak $I_{K\text{-}LVA}$ vs. open-tip pipette resistance. Average currents for patches recorded with 8 and 9 MΩ electrodes were not significantly different (Student's t-test, p=0.26, n=25 and 10, respectively). **b.** There was no systematic difference in pipette resistance as a function of dendritic recording distance. Data were grouped into 20 μm bins. Linear fit: =0.002 MΩ/μm.